LOCAL MECHANICAL AND MICROSTRUCTURAL CHARACTERIZATION OF ELECTRON BEAM WELDED 15-5PH STAINLESS STEEL

E. Herny[1, 2], P. Lours[2], J. M. Cloue[1], P. Lagain[3], S. Perusin[1], E. Jourdain[2] and E. Andrieu[1]

[1] Ecole Nationale supérieure des Ingénieurs en Arts Chimiques et Technologiques, Laboratoire du CIRIMAT (Centre Interuniversitaire de Recherche et d'Ingénierie des MATériaux) UMR5085 CNRS, 118 route de Narbonne, 31077 Toulouse cedex 4, France.

[2] Ecole des Mines d'Albi-Carmaux, Laboratoire du CROMeP (Centre de Recherche Outillages, Matériaux Et Procédés) Route de Teuillet, 81013 Albi Cedex 9, France.

[3] Airbus Industrie, site de St-Martin, 316 Route de Bayonne, 31300 Toulouse, France.

HOME

ABSTRACT

Aged hardened martensitic stainless steels are basically low carbon, high chromium and nickel steels. They are characterized by high strength and toughness combined with a good corrosion resistance. In the 15-5PH stainless steel, the mechanical strength is due to the precipitation of copper rich phases, the toughness is optimised by controlling the volume fraction of reversed austenite while the corrosion resistance is attributable to the high chromium content. The 15-5PH has been reported to be readily weldable and weldments generally show good mechanical properties.
The present study is conducted to investigate the mechanical and metallurgical properties of electron beam welded 15-5PH alloy. The fusion zone has a dendritic microstructure and subsequently to welding, heat affected zone (HAZ) extends on both sides of the fillet. The HAZ shows a different microstructure compared to both the molten zone and the base metal. To investigate the mechanical properties, tensile specimens are extracted from the various zones of the welded junction in order to characterize the local properties of the heat-affected zone (HAZ) and the fusion zone (FZ) and to compare them to those of the base metal.

KEYWORDS

Stainless steel, reversed austenite, copper precipitation, electron beam welding, microstructure, differential thermal analyses.

INTRODUCTION

Precipitation hardening (PH) martensitic stainless steels are used in aerospace and nuclear industries, where they are usually subject to high stress. Good mechanical properties are thus required for those applications. Because of the low carbon content, the matrix has to be hardened by a standard solutionizing, quenching and tempering treatment. A low addition of copper results in significant hardening through the precipitation of Cu rich particles occurring during tempering. Together with this precipitation, the reversion of the martensite leads to the formation of a few percents of austenite called reversed austenite.
Generally speaking, martensitic stainless steels exhibit good weldability. Several studies have been reported in the literature focussing on the evolution of the weld microstructure of PH stainless steels [1, 2, 3, 4].
The present study aimed at characterizing microstructural evolution as well as associated mechanical properties induced by an electron beam welding of 15-5PH stainless steel followed by tempering at 550 °C during 4 hours. Several analytical techniques were used for this purpose. Among them, differential thermal analyses were performed to determine the different phase transformations occurring during the tempering treatment of both the base metal and the welded metal together with microstructural observations by TEM. The local tensile properties of the fusion zone, of the heat affected zone and of the base metal were measured at room temperature and related to the microstructure of the various zones.

MATERIAL AND EXPERIMENTAL DETAILS

The overall thermal treatment of the alloy, whose composition is given table 1, consists in:

- solution heat treatment at 1050 °C for 30 minutes
- air quench
- tempering at 550 °C for 4 hours with a heating rate of 2.5 °C.min^{-1}.

Table 1: Chemical composition of 15-5PH (wt%)

Element	C	Si	Mn	S	P	Ni	Cr	Mo	Cu	Nb	Ta	Fe
wt %	0,022	0,38	0,8	<0,002	0,015	4,91	14,83	0,25	3,02	0,19	<0,05	balance

Welding is conducted straight after quenching and the specimens obtained are subsequently aged at 550 °C during 4 hours.
For both base metal and welded metal, the heat treatment promotes the precipitation of coherent Cu particles and the formation of reversed austenite within the martensite matrix, thus providing a satisfactory compromise between strength and toughness.
Specimen's microstructures are first examined with an optical microscope after different etchings for general observations. Transmission electron microscope (TEM) observations are then carried out using a JEOL^{TM}2010 operating at 200 kV. Thin foils for TEM are gound down to 60 µm thick then twin-jet electropolished using a 5 % perchloric acid-acetic acid solution at 15 °C.
The differential thermal analysis (DTA) is conducted in a Setaram Setsys 16/18 apparatus with a pan system holding the investigated sample and pure aluminium as reference. Both pans are exposed to the same heat source under a continuous argon flow. The temperature difference is measured and reveals exothermic and endothermic transformations.
Specimens for tensile tests are extracted from various zones, namely the base metal, the heat affected zone (HAZ) and the fusion zone (FZ). The choice of the specimen thickness is constrained by the thickness of the fusion zone, which is 1.5 mm. Indeed, this zone is the thinnest of the three domains. In order to extract two specimens and be sure to investigate precisely the fusion zone, the thickness of the specimens is decreased down to 500 µm. This geometry is adopted for the whole bench of specimens cut from the base metal and from the HAZ. Tensile experiments are performed using a MTS electromechanical machine with a load cell of 5000 N and a strain rate of 10^{-3} s^{-1}.

MICROSTRUCTURAL INVESTIGATION

A- TEMPERED BASE METAL

Figure 1 shows a bright field TEM image of the alloy after tempering. Both Cu precipitates, roughly spherical and about 10 nm large, and reversed austenite are clearly observed within the martensite laths. The reversed austenite is easily identified by its typical high nickel content revealed by energy dispersion spectroscopy analysis (EDS). This reversed austenite may also form in the lath boundaries (not shown here).
Note the presence of niobium carbides of about 100 nm in the martensite. Niobium is incorporated in the material because of its high affinity with carbon. This prevents the precipitation of chromium

carbides which would lead to a Cr depletion in the matrix and provoke a loss of corrosion resistance.
The Cu precipitates are face centred cubic as well as the reversed austenite. Their crystalline structures present the Kurdjumov and Sachs (K-S) orientation relationship with the body centred cubic matrix [5, 6].

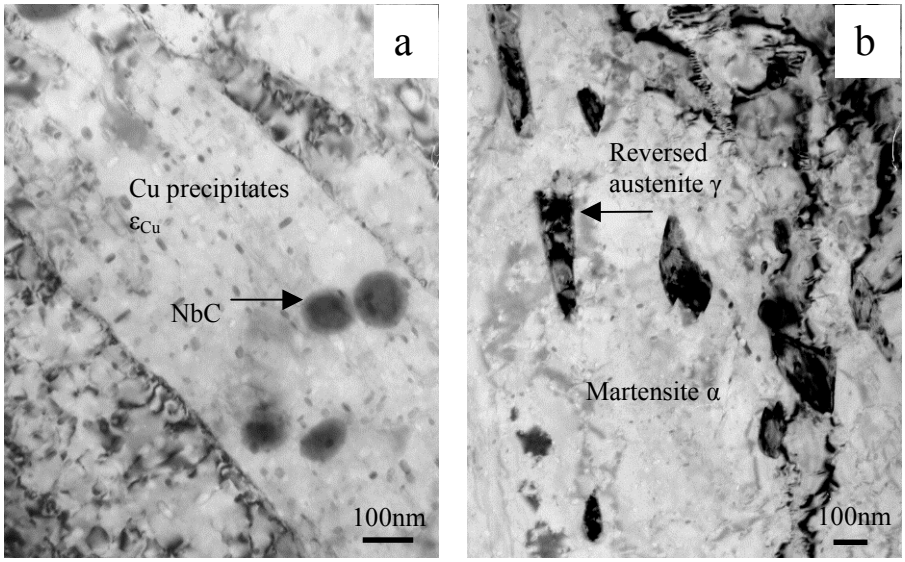

Fig. 1: a) TEM micrograph showing Cu precipitates; b) TEM micrograph showing reversed austenite

Differential thermal analysis has been performed on the base metal before the aging treatment up to 1050 °C with a heating and cooling rate of 5 °C/min. In addition, the same experiments are performed on the tempered material. Curves can be readily distinguished. Copper precipitation must show up only on the data characteristic of the solution heat treated material. Precipitation is assumed to be at least partially completed in the tempered alloy.
Indeed, as shown in Figure 2 a and b, the solution heat treated material exhibits first an exothermic peak corresponding to the precipitation of copper and then an endothermic peak characteristic of the reversion of the martensite. As expected, the tempered sample only shows the endothermic transformation.

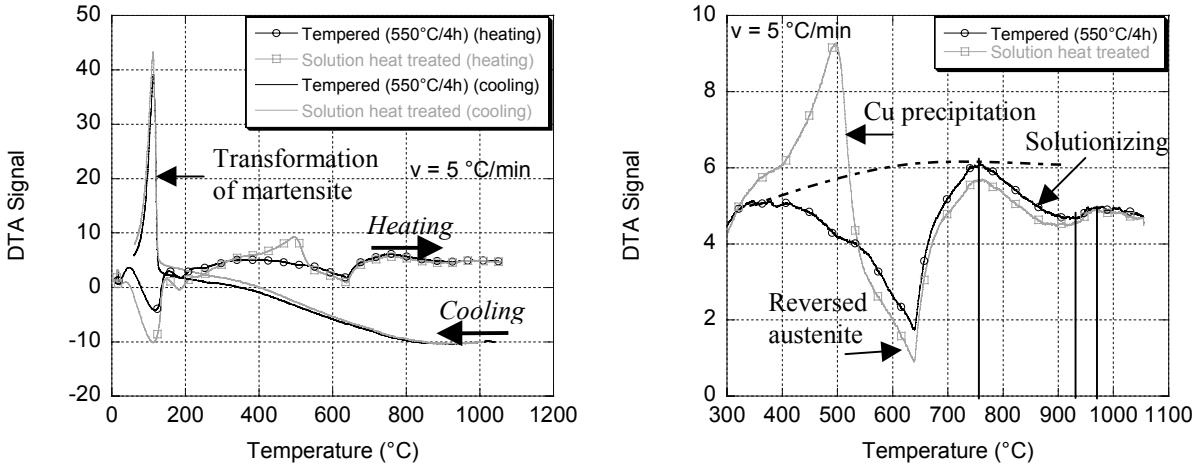

Fig. 2: a) DTA of the solution heat treated and the tempered specimens; b) Detail of the heating part

HOME

Once copper precipitation is completed, above 550 °C, both curves are strictly equivalent.
The dashed curve in figure 2b indicates the possible base line if no phase transformation occurs. The endothermic transformation, starting at 750 °C, corresponds to the solutionizing of the copper precipitates. This solution annealing is achieved at 925 °C, few tens of degrees before the completion of the austenite transformation at about 960 °C.
Oscillations, at the beginning of heating, correspond to instabilities due to the machine, before the stationary state. The final exothermic peak at the end of cooling corresponds to the start of the martensite transformation at a Ms temperature close to 120 °C.
To study the influence of the heating rate on the phase transformations in the solution heat treated alloy, differential thermal analyses were carried out with heating rates in the range 2.5 °C.min^{-1} to 30 °C.min^{-1}. Figure 3 shows the curves obtained during heating to 400°C until 1050°C for the different heating rates.

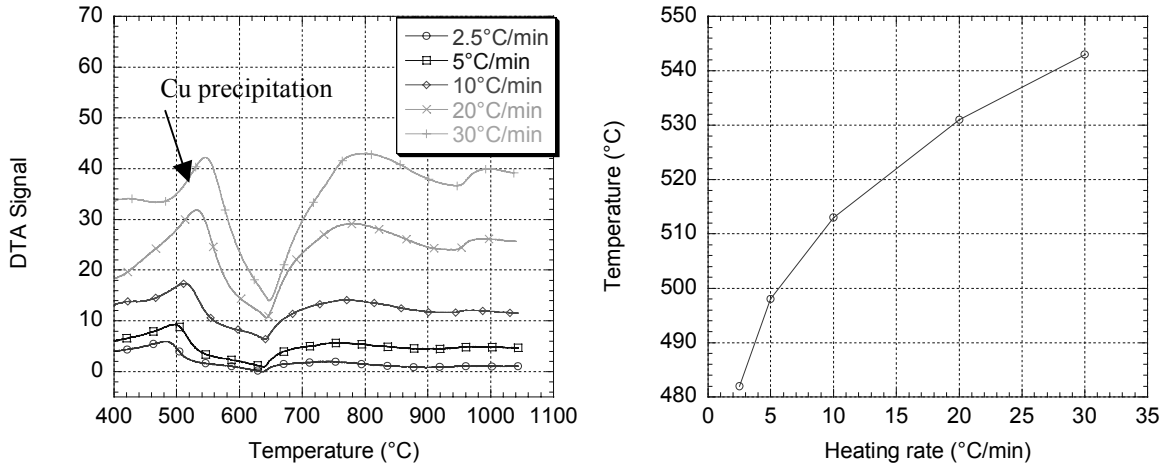

Fig. 3: a) DTA of the solution heat treated samples at different heating rates; b) Peak temperature for Cu precipitation versus heating rate

The peak temperature for copper precipitation changes with the heating rate, v, the higher the heating rate, the higher the temperature. The evolution allows to determine the activation energy of the phase transformation. The activation energy is calculated using the Kissinger method [7] by plotting ln(v/Tm²) versus (1/Tm), with Tm the peak temperature (figure 4). The slope corresponds to (-Q/R) leading to an activation energy of about 197 kJ/mole. This value is higher than that obtained by Wiswanathan [8] (Q =112 kJ/mole) for the precipitation of copper in alloy 17-4 PH. This discrepancy might be due to the difference in dislocation density that may be higher in alloy 17-4PH thus hindering the transformation.

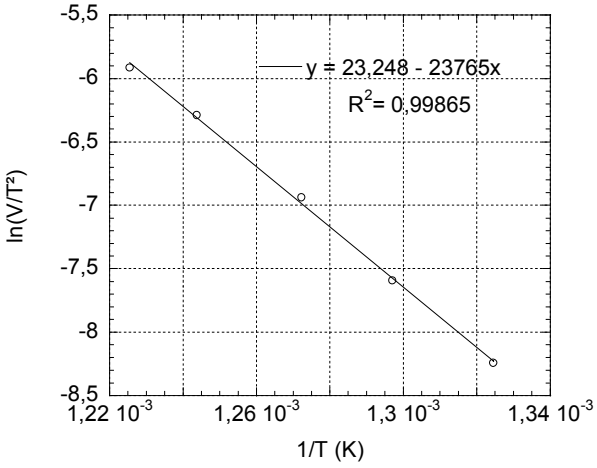

Fig. 4: Arrhénius plot of Ln(v/Tm²) versus 1/T and estimation of the activation energy for Cu precipitation

To approach the microstructural evolution during welding, differential thermal analysis has been performed for the solution heat treated material up to the melting point. All the transformations occurring during melting of the alloy are detailed in figure 5.

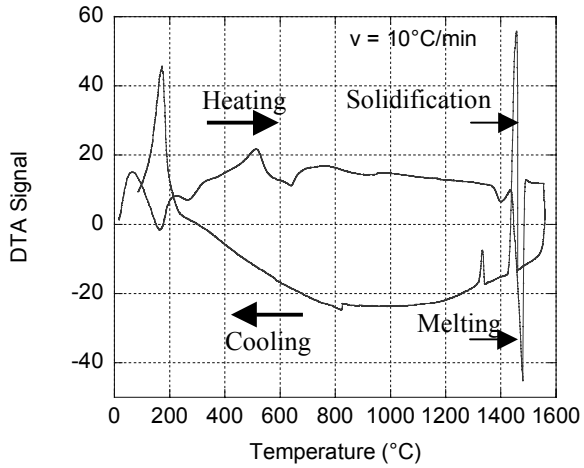

Fig. 5: DTA of the solution heat treated alloy up to complete melting

Melting starts at 1430 °C and finishes at 1480 °C as indicated by the endothermic peak. Reverse transformation (solidification) occurs upon cooling. In addition, the precipitation of niobium carbides is revealed upon the cooling by the occurrence of the exothermic peak at a temperature of 1346 °C.

B- TEMPERED WELDED METAL

The electron beam welding process is carried out with an advance of 12 mm/s. The cooling rate of the material and consequently the microstructure depend on the distance of the considered zone with respect to the axis of the electron beam pass. For instance, the central zone is melted as the electron beam impacts the material surface and is subject to a very high cooling rate. In this zone,

the solidification is dendritic, the dendrite arms being highly elongated in the direction of the heat flux established during solidification.
Figure 6a shows a general macrograph of the electron beam welded 15-5PH alloy. While processing, a 1.5 mm thick central zone is melted (FZ). On both sides of the fillet, a heat affected zone (HAZ) extends over 3 mm (figure 6b, c, d).

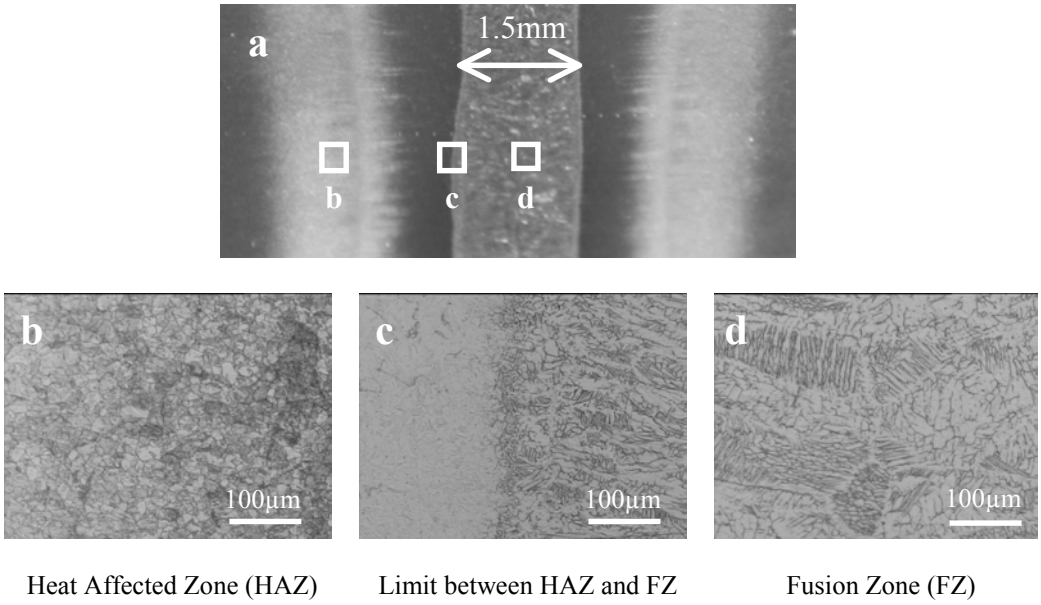

Fig. 6: a) Macrograph of the welded junction; b) Micrograph of HAZ; c) Micrograph of the interfacial region between the molten zone and the heat affected zone; d) Micrograph of the FZ

The FZ exhibits a typical solidification dendritic structure. Grain size in the HAZ and the base metal is respectively about 20 µm (figure 6b) and 30 µm. Note that etching reveals a dark band at the extremity of the both HAZ commonly referred to as the far heat affected zone.

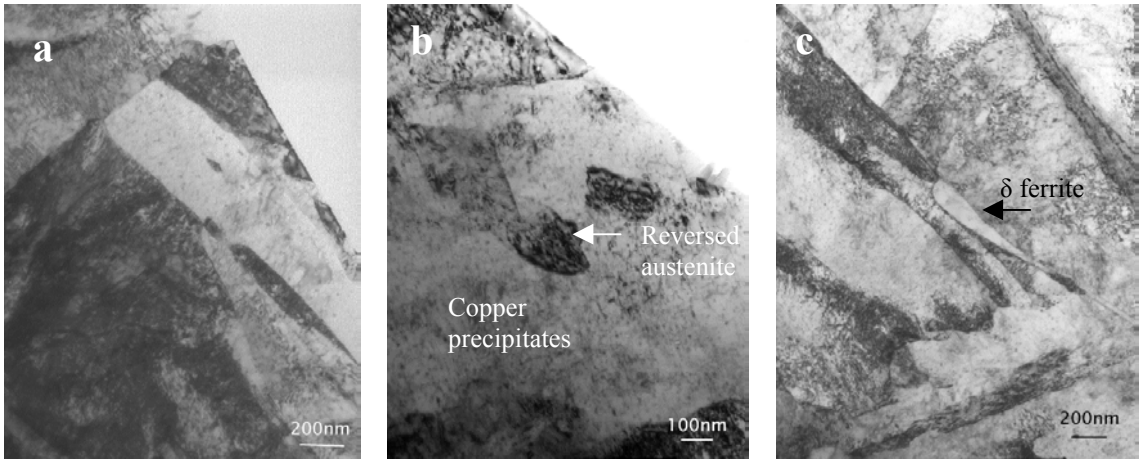

Fig. 7: TEM micrographs of the fusion zone showing, Cu precipitates within martensite laths (a), reversed austenite and copper precipitates (b) and δ ferrite (c)

Figures 7a, b & c show TEM bright field images of the fusion zone after tempering taken in different areas of the specimen. High nickel reversed austenite (figure 7b) as well as high chromium

delta ferrite (figure 7c) can be observed and are formally identified by coupling TEM and EDS analysis [9]. This delta ferrite nucleates and grows during the solidification. Its volume fraction depends on various parameters such as the cooling rate and the chemical composition of the material. If present in the alloy in moderate quantity, this phase, intrinsically ductile, may avoid hot cracking during the welding process

Similarly to the base metal, the heat affected zones present martensite laths and reversed austenite. However, no delta ferrite is observed in the HAZ. To address the occurrence of any phase transformation during thermal treatment, differential thermal analysis performed on the fusion zone and the heat affected zones prior to tempering, are in progress.

TENSILE PROPERTIES

Room temperature tensile tests have been performed to determine the local mechanical properties of the material in the various representative regions issued from the welding process: base metal, heat affected zone and fusion zone.

The necessity to machine specimens, as thin as 500 µm, has been discussed previously. It is quite unusual to work out such type of geometry for tensile testing. As a consequence, the possible influence of the specimen thickness on the results of the tensile tests has been studied in the case of the tempered base metal. Measurement of the specimen must be thoroughly conducted as a small error in estimating the thickness (30 µm) can lead to large mistake in the calculation of the stress (60 MPa). Figure 8 shows the response of the different specimens with various thicknesses ranging from 184 µm to 1230 µm. All plots can be perfectly superimposed in the whole elastic domain and up to the beginning of necking as long as strain is homogeneously distributed in the specimen. The Young modulus (196 GPa), yield strength (1100 MPa) and ultimate tensile strength (1150 MPa), are basically independent of the specimen thickness. In each case, note that no or very little work-hardening occurs. The elongation to rupture decreases with the specimen thickness from 14.5 % to 6.5 %, which might be simply attributed to an effect of the progressive reduction of the specimen cross-sections consequently restricting the possibility for post-necking deformation.

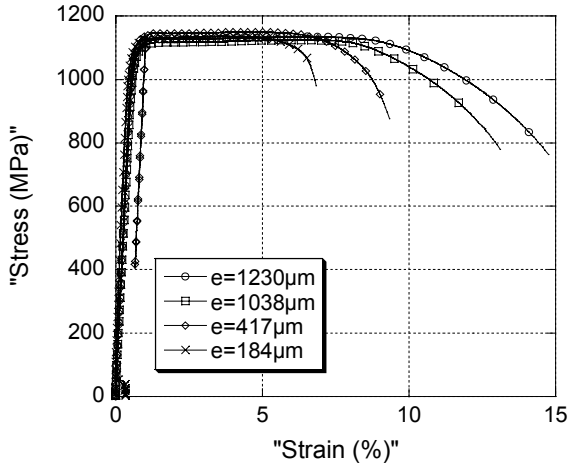

Fig. 8: Stress-strain plots of the tempered base metal as a function of specimen thickness

After welding, specimens are tempered (550 °C for 4 hours). Figure 9 compares the characteristic obtained locally in the fusion zone (FZ), the heat affected zone (HAZ) and the base metal.

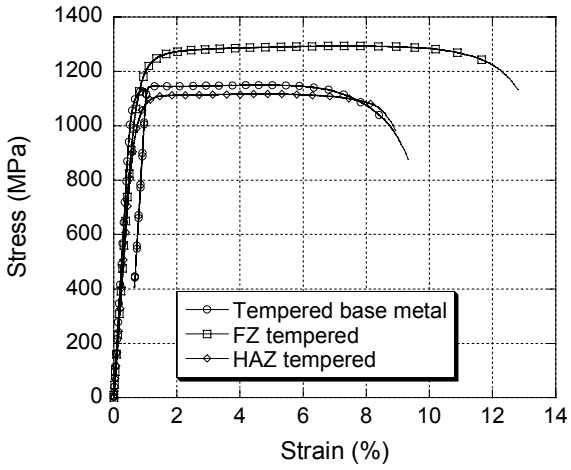

Fig. 9: Comparative stress-strain plots for the FZ, HAZ and the base metal

The slope of the elastic domain from which the Young modulus can be derived is very similar from one zone to the other. The fusion zone shows superior resistance (yield strength 1196 MPa) than the base metal which in turn is slightly more resistant than the heat affected zone (1054 MPa). Additional complementary Vickers hardness tests confirm this tendency.

To understand the difference in tensile properties between the base metal, the fusion zone and the heat-affected zone, it is necessary to consider the thermal history of the three regions. This thermal history directly dictates the microstructure of the material.

As described previously and because of the high temperature and high cooling rate involved, the fusion zone is essentially dendritic with elongated grains and some delta ferrite. The grain size in this zone is quite low around 15 µm. The heat-affected zones are sufficiently thick to see a temperature gradient. This temperature gradient through out the HAZ ranges from the melting temperature to a temperature below which no phase transformation is likely to occur. This temperature may be formally fixed around 450 °C corresponding to the temperature where copper particles begin to precipitate.

The temperatures corresponding to the start and finish of the austenite transformation Ac1 and Ac3 lie within this temperature range. Figure 10 is an attempt to model, regarding the thermal history of a typical welded specimen, the type of microstructure temporary obtained while processing EB welding. It is assumed that this temporary structure will generate the microstructure obtained after final return to room temperature following the completion of welding. The HAZ material will be martensitic after return to room temperature but will show slightly different grain sizes depending on the HAZ sub-zones considered, that is the temperature seen.

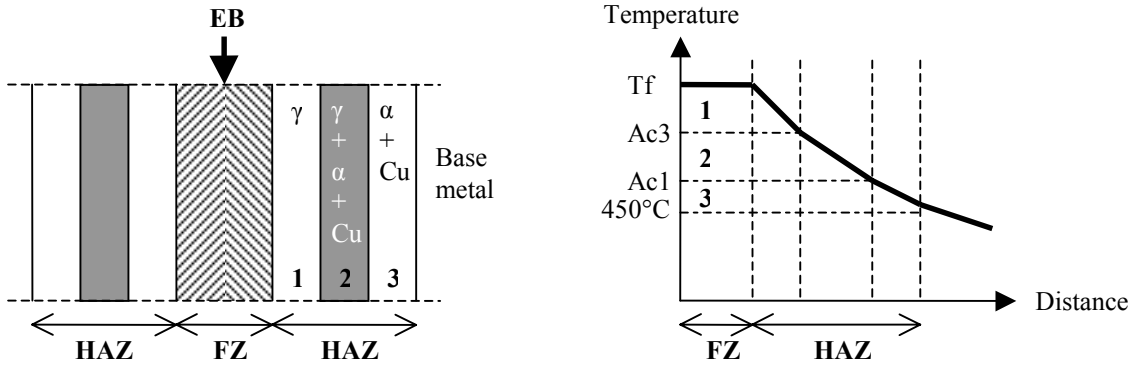

Fig. 10: Schematic representation of the different zones of the material during welding and corresponding temperatures

Close to the fusion zone, the metal is entirely austenitic down to the temperature Ac3. In this temperature range, the grain size increases compared to the base metal (sub-zone 1). Between Ac3 and Ac1, the microstructure is a mix of austenite, martensite and copper precipitates (sub-zone 2). In this domain, grains refine down to a size smaller than that in the base metal. Below Ac1, the metal remains martensitic with copper precipitation. This microstructure is prevalent within a domain heated above 450 °C. Beyond, the temperature is too low to promote any copper precipitation (< 450 °C).
It is well known that the mechanical properties directly depend on the microstructure. The FZ tensile properties are higher than that of the base metal and the HAZ because it microstructure is finer and because the delta ferrite becomes hardened after tempering. Indeed, the delta ferrite has high chromium content and during the tempering this ferrite demixed in a chromium rich phase (very brittle) and in an iron rich phase. This phenomenon can explain why the FZ tensile properties are so high.
The HAZ shows the lowest tensile resistance. As discussed above, the HAZ is divided in three sub-zones, each one exhibiting specific grain size. Regarding the values of the yield strength it is assumed that the specimen was extracted from the sub zone 1, where the grains grow too largely prior to tempering.

CONCLUSION

The microstructure of 15-5 PH alloy and electron-beam welded 15-5 PH alloy has been investigated.
In the as tempered material, MET observations reveal the presence of niobium carbides, copper precipitates and reversed austenite located either within the martensite laths or in the laths boundaries. Those phases give to the alloy the best compromise between strength and toughness. Differential thermal analysis performed on the solution heat-treated metal prior to tempering allows to determine the activation energy of the copper precipitation.
During welding, the stainless steel undergoes many phases transformation in the central zone melted by the electron beam and the so-called heat affected zones. The fusion zone exhibits a typical dendritic structure containing delta ferrite. The heat affected zones are subject to a thermal gradient where temperature drops from the melting temperature of the material to the temperature of copper precipitation. As a consequence, the microstructure of the heat affected zone exhibits various grain size changing throughout its thickness.
Tensile tests, performed on specimens extracted from the fusion zone, the heat affected zone and the base metal, show that the fusion zone has superior resistance. It is assumed that the presence of delta ferrite that demixes upon tempering is essentially responsible for this. This phenomenon occurs in stainless steel with high chromium content during aging and is very detrimental for the impact strength energy.
For a better understanding of demixtion and its impact on the mechanical properties of the material, further work is in progress to study the metallurgical effect of aging. This will be carried either purely thermally with no stress or under combined and controlled conditions of stress and temperature.

ACKNOWLEDGEMENTS

The authors wish to acknowledge the contribution of J. Lacaze for performing the differential thermal analyses and M. C. Lafont for TEM observations.

REFERENCES

1) J. A. BROOKS and J. W. M. GARRISON, Welding Research Supplement, (1999), p 280.
2) K. OZBAYSAL and O. T. INAL, Materials Science and Engineering, A130, (1990), p 205.
3) J. M. WRIGHT and M. J. JORDAN, Metals Technology, (1980), p 473.
4) K. OZBAYSAL and O. T. INAL, Journal of Materials Science, 29, (1994), p 1471.
5) H. R. HABIBI BAJGUIRANI, Materials Science and Engineering, A338, (2002), p 142.
6) H. R. HABIBI BAJGUIRANI, C. SERVANT and G. CIZERON, Acta Metallurgical Material, 41, (1993), p 1613.
7) J. M. CLOUE, thèse, Ecole des Mines de Paris, PARIS (1998).
8) U. K. VISWANATHAN, P. K. K. NAYAR and R. KRISHNAN, Materials Science and Technology, 5, (1989), p 346.
9) M. J. CIeslak, C. R. HILLS, P. F. HLAVA and S. A. DAVID, Metallurgical Transactions A, 21A, (1990), p 2465.